applied sciences

MDPI

Article

Experimental Investigation and Theoretical Simulation of Resistivity Response to Relative Permeability Variation

Zhihua Guo [1,2], Qi Fan [1,2], Yuhao Li [3], Zongli Liu [1,2] and Yang Zhao [4,5,*]

[1] College of Geo-Science, Northeast Petroleum University, Daqing 163318, China; guozhihua@nepu.edu.cn (Z.G.)
[2] Key Laboratory of Continental Shale Hydrocarbon Accumulation and Efficient Development, Ministry of Education, Northeast Petroleum University, Daqing 163318, China
[3] Daqing International Exploration and Development Company, Daqing 163318, China
[4] College of Petroleum Engineering, Northeast Petroleum University, Daqing 163318, China
[5] Laboratory of Enhanced Oil Recovery of Education Ministry, Daqing 163318, China
* Correspondence: dqzy0683@163.com

Featured Application

This study establishes a comprehensive experimental database of relative permeability–resistivity joint measurements based on artificial core samples pressed under simulated reservoir conditions, with parameters covering reservoir physical properties, fluid occurrence characteristics, and mineral compositions. A relationship model is developed to estimate oil–water relative permeability from resistivity data for complex argillaceous sandstone reservoirs bearing conductive minerals. The model enables the prediction of relative permeability using electrical parameters such as resistivity, providing a novel theoretical basis and technical pathway for the identification of low-resistivity pay zones and the evaluation of reservoir productivity.

Abstract

Oil–water relative permeability is a critical parameter for reservoir fluid property evaluation and productivity prediction, playing a vital role in reservoir identification and development. However, the correlation between relative permeability and resistivity remains unclear for complex conductive mineral-bearing argillaceous sandstone reservoirs. In this study, twenty-eight artificial core samples were prepared and compacted under simulated reservoir temperature and pressure conditions. Simultaneous oil–water relative permeability and resistivity measurements were performed on these samples at two brine salinities (7000 ppm and 3000 ppm). The analysis reveals that under the same resistivity index, both conductive-mineral content and shale content exhibit a negative correlation with water-phase relative permeability but a positive correlation with oil-phase relative permeability. In contrast, porosity–permeability conditions and injected-water salinity show a positive correlation with water-phase relative permeability and a negative correlation with oil-phase relative permeability. Furthermore, the effect of salinity on the relative permeability–resistivity relationship intensifies as porosity–permeability conditions improve. Based on the consistency between movable water seepage and conductive paths, a novel relative permeability–resistivity model was developed for the target reservoirs by integrating seepage and conductive theories, with a generalized Archie's equation adopted to calibrate the effects of conductive minerals and shale on rock conductivity. The model parameters are optimized using the Newton–Raphson iteration algorithm, and empirical correlations between the undetermined coefficients and reservoir parameters are developed. Validated against two independent cores with the most complex mineral compositions (SH2-3 and SH3-3), the model yields average relative errors of 9.8%

Check for updates

Academic Editor: Kun Sang Lee

Received: 24 July 2026
Revised: 26 August 2026
Accepted: 26 August 2026
Published: 29 August 2026

Copyright: © 2026 by the authors. Licensee MDPI, Basel, Switzerland. This article is an open access article distributed under the terms and conditions of the Creative Commons Attribution (CC BY) license.

and 13.4% for water-phase relative permeability, and 4.4% and 5.4% for oil-phase relative permeability, respectively, demonstrating its high calculation accuracy. It enables efficient prediction of reservoir relative permeability using resistivity data, providing a new theoretical and technical support for low-resistivity oil reservoir identification and productivity assessment.

Keywords: relative permeability; experimental design; experimental characterization; theoretical simulation

1. Introduction

Oil–water relative permeability is a critical parameter governing multiphase flow in reservoir evaluation, production forecasting, and development strategy optimization. Its accurate determination directly influences reservoir performance and the ultimate potential for enhanced oil recovery. As a routinely acquired parameter in well logging, resistivity responses are directly related to pore fluid distribution and occurrence states, and can indirectly reflect multiphase flow capacity. Therefore, revealing the relationship between oil–water relative permeability and resistivity, and establishing phase-permeability inversion equations based on electrical responses holds significant theoretical importance and engineering application value for achieving low-cost, continuous evaluation of reservoir seepage parameters.

From a fundamental rock-physics perspective, the response characteristics of both permeability and electrical resistivity are influenced by pore-space geometry. According to Kobranova [1], the effective permeability of reservoir rocks is proportional to the square of pore diameter and inversely proportional to the tortuosity of fluid-flow pathways. In contrast, resistivity is governed by porosity, pore-space tortuosity, pore-fluid conductivity, and the presence of clay minerals [2–5]. Although porosity and tortuosity affect both permeability and resistivity, their influences on the two parameters are not identical. Moreover, permeability is additionally controlled by the diameter of fluid-conducting channels—a parameter that does not appear in the Archie equation. Consequently, two porous media with identical porosity but different pore tortuosity or pore-throat sizes may exhibit similar resistivity yet markedly different permeability. This intrinsic disparity fundamentally explains why permeability cannot be reliably estimated from resistivity data alone. Regarding the study of the relationship between relative permeability and resistivity, domestic and international scholars have conducted systematic research in multiple directions and achieved corresponding progress. In the direction of establishing relative permeability–resistivity models for pure sandstone, since Archie established the resistivity equation for pure sandstone, researchers have developed a fundamental inverse-relationship model between wetting-phase relative permeability and resistivity index based on the similarity between fluid seepage and electrical current conduction [6,7]. Subsequent modifications addressing pore structure heterogeneity, unsteady-state experimental errors, wettability, and other factors have led to methods including unsteady-state relative permeability resistivity correction, relative permeability calculation for complex pore structures, and resistivity dynamic inversion [8–14], which have achieved good application results in conventional pure sandstone reservoirs. In the direction of conductivity and relative permeability correction for shaly sandstone, classical shaly sandstone conductivity models such as the Waxman–Smits model and the dual-water model have been successively established to address the challenge of shale additional conductivity [2–5]. In addition, Koelman and de Kuijper [15] proposed an effective-medium model capable of describing the anisotropy and electrical conductivity of multi-component mixtures, providing a general theoretical

formulation for calculating the resistivity of rocks whose matrix contains conductive minerals. Subsequently, Glover [16] generalized the Archie equation to an N-phase form, which has since been applied to rocks containing pyrite and other complex mineral assemblages. In the direction of electrical conductivity characteristics of rocks containing conductive minerals, scholars have clarified through experiments and numerical simulations the influence patterns of conductive mineral content and distribution on rock electrical parameters, confirming that connected conductive mineral networks reduce rock resistivity, and that interfacial polarization effects can produce unique dispersion characteristics, which are important causes of low-resistivity reservoirs [17–21]. In the direction of pore structure research, fractal theory has been widely used for quantitative characterization of pore heterogeneity, and researchers have established fractal porous media relative permeability and resistivity index models, multifractal resistivity models, and combined these with nuclear magnetic resonance technology to achieve quantitative pore structure characterization and direct calculation of relative permeability parameters [22–28]. Pape et al. developed a fractal pore-space model that establishes the relationships among porosity, tortuosity, and permeability across the entire sandstone spectrum [29]. Zisser et al. demonstrated that spectral induced-polarization relaxation time correlates with hydraulic permeability through an effective pore-length scale [30]. In the field of digital rock physics, Bakke et al. pioneered three-dimensional pore-scale reconstruction and fluid flow simulation in sandstones [31]. Bultreys et al. and Gharbi et al. simulated water-flooding processes in heterogeneous rocks with variable wettability using multiscale pore-network models [32,33]. Nuclear magnetic resonance (NMR) methods, often integrated with digital rock techniques, have enabled the direct estimation of absolute and relative permeability from relaxation-time distributions [34]. In terms of intelligent prediction, machine learning and deep learning approaches—including neural networks [35], transformer-based models [36], and particle-swarm-optimized inversion [37]—have been applied to estimate relative permeability parameters from well-log data.

In terms of experimental techniques and artificial cores, the development of high-temperature high-pressure artificial core preparation and digital core technologies has enabled the fabrication of artificial cores with controllable pore structures and simultaneous multi-parameter testing [38–40]. In the direction of salinity effects and intelligent prediction, researchers have clarified the influence of formation water salinity on wettability and relative permeability parameters. Despite the significant advances achieved in existing studies, several research gaps remain. Existing multi-component resistivity models can accurately describe the resistivity of rocks containing conductive minerals, but they do not establish a direct transformation between resistivity and relative permeability [15,16,41]. Digital rock and nuclear magnetic resonance (NMR) methods [31–34] can compute relative permeability from pore-scale images or relaxation data; however, they require high-resolution imaging data or core samples, which are not routinely available from conventional well-logging measurements. Machine learning models [35–37,42] offer empirical predictive capability but generally lack explicit physical constraints linking conductive theory to two-phase flow mechanisms. In terms of experimental design, few studies have reported simultaneous relative permeability and resistivity measurements on core samples that systematically account for multi-factor variations in porosity, clay content, conductive-mineral content, and formation-water salinity.

To address the limitations of existing studies discussed above, this paper conducts experimental analysis and theoretical simulation studies on the relationship between oil–water relative permeability and resistivity. The novelty of this work is threefold. First, multiple groups of core samples with gradient variations in porosity, permeability, shale content, and conductive mineral content are fabricated, and oil–water relative permeability–resistivity

simultaneous measurements and supporting parameter experiments are conducted under strictly controlled temperature and pressure conditions, establishing a simultaneous measurement experimental data system covering multiple key parameters. Second, the single-factor influences and variation patterns of pore structure, conductive minerals, shale content, and formation water salinity on seepage and conductivity characteristics are analyzed. Third, a generalized Archie conductivity correction was coupled with a relative permeability transform model based on the geometric similarity between movable-water conductive paths and seepage pathways, leading to the development of a relative permeability–resistivity correlation model applicable to complex shaly sandstones containing conductive minerals, with its prediction accuracy rigorously validated. The results demonstrate that the model coefficients correlate systematically with measurable reservoir parameters, thereby providing a calibration pathway for field applications. The research findings of this paper aim to provide theoretical support and experimental evidence for relative permeability evaluation of such reservoirs.

2. Materials and Methods

Oil–water relative permeability is a core parameter for evaluating reservoir fluid production characteristics and predicting productivity, and it holds significant practical importance for the identification and development of complex reservoirs caused by factors such as conductive minerals and shale content. In view of the current unclear understanding of the relationship between relative permeability and resistivity in complex argillaceous sandstone reservoirs containing conductive minerals, this paper systematically investigates the intrinsic relationship between the two from an experimental perspective, based on simultaneous measurements of relative permeability and resistivity along with supporting experiments. In the simultaneous measurement experiments of oil–water relative permeability and resistivity, multiple geological and petrophysical parameters collectively influence the seepage characteristics and electrical conductivity of rocks. To address this, this study designed and fabricated various types of artificial core samples, systematically varying their porosity-permeability structure, clay content, and conductive mineral content ratios. Under rigorously controlled laboratory conditions, a series of systematic seepage-resistivity simultaneous measurement experiments were conducted, yielding reliable fundamental data.

First, to overcome the limitations of natural cores—which are difficult to artificially control in terms of composition, structure, and mineral content—this study simulates actual reservoir temperature and pressure conditions, using natural mineral particles as raw materials, and systematically designs and fabricates multiple groups of artificial core samples with different porosity-permeability structures, conductive mineral contents, and shale contents (Figure 1), in order to quantitatively investigate the influence of each factor on oil–water relative permeability and resistivity. The use of artificial core samples in experimental investigations of seepage and electrical conductivity enables effective isolation and quantitative evaluation of the independent contributions of individual reservoir parameters to rock electrical and flow properties. On this basis, a series of systematically designed artificial core experiments was conducted in this study, in which each experimental group was configured with a single reservoir parameter varying while the others were maintained approximately constant. This experimental strategy provides a reliable foundation for the screening and determination of key parameter variables in the subsequent model development. Regarding the selection of conductive mineral types, full consideration was given to the actual geological conditions of major oilfields. Pyrite, being the most widely distributed and commonly occurring conductive mineral in natural reservoirs, was chosen as the representative conductive mineral in this investigation. Accordingly, the

core samples designated as P1, P2, SH2, SH3, and SH4 employed in this study were all fabricated using pyrite particles of varying mesh sizes, compacted under different mass proportioning schemes. The measured electrical conductivities of the conductive mineral fraction and the shale fraction in this series of core samples are approximately 0.2 S/m and 0.5 S/m, respectively.

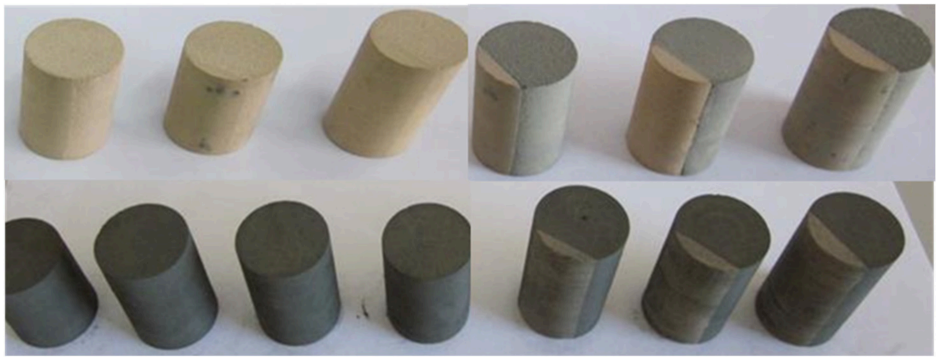


Figure 1. Photographs of artificially compacted samples from complex lithological formations.

Secondly, to systematically investigate the response relationship between oil–water relative permeability and resistivity, this study sequentially conducted multiple petrophysical property measurements on various core samples: porosity and permeability were determined using a CM-300 measurement system; irreducible water saturation (S_{wi}) was obtained using a GeoSpec2 NMR core analyzer (Oxford Instruments, Buckinghamshire, UK); steady-state relative permeability and resistivity simultaneous measurement data were acquired using an XYS-3 relative permeability–resistivity simultaneous measurement system (Figure 2); and the relative contents of various mineral components in the rock samples were determined using a MASTERSIZER-2000 laser particle size analyzer (MASTERSIZER, Worcestershire, UK). All reported data for each experiment represent averaged values from multiple measurements to ensure accuracy and repeatability.



Figure 2. XYS-3 relative permeability measurement system.

Furthermore, to simulate the influence of formation water salinity variations on reservoir seepage and electrical conductivity characteristics during oilfield development,

two sets of comparative displacement experiments were designed in this study: (1) simultaneous relative permeability–resistivity measurements were conducted under conditions where both the initial saturation water and injected water had a salinity of 7000 ppm (the experimental procedure is illustrated in Figure 3). (2) While keeping all other conditions unchanged, the injected water salinity was reduced to 3000 ppm, and the above experimental procedure was repeated to simulate the common freshwater flooding process encountered in oilfield production. The selection of the two arbitrary salinity points (7000 ppm and 3000 ppm) in this study was based on the actual conditions of original formation water and freshwater flooding in oilfield development. The 7000 ppm level is representative of the typical original formation-water salinity in many continental sandstone reservoirs (e.g., the Daqing Oilfield), whereas the 3000 ppm level approximates the salinity of injected water or treated produced water during freshwater flooding. This contrast satisfies the requirements for analyzing the resistivity and relative-permeability responses during both edge/bottom-water encroachment and freshwater-flooding processes encountered in field production. The steady-state relative-permeability measurements in this study strictly followed standard procedures, requiring multiple parameters to simultaneously satisfy the steady-state criteria: (i) consecutive readings of pressure differential across the core showed relative deviations of less than 3% without systematic drift; (ii) the effluent oil and water production rates were stable and consistent with the injection rates; and (iii) the water saturation inside the core, calculated by the material-balance method, remained controllable and no longer varied with time.

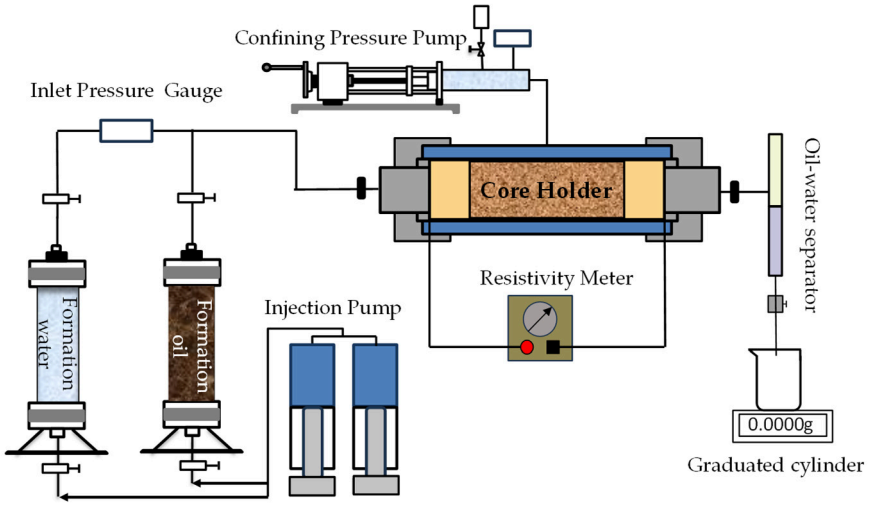


Figure 3. Experimental workflow for relative permeability–resistivity joint measurement.

The experimental scheme and workflow designed in this study not only enable a comprehensive and systematic analysis of the influences of reservoir pore structure, conductive minerals, shale content, and formation water salinity on the oil–water relative permeability–resistivity relationship, but also provide a basis for further revealing the underlying mechanisms. This lays the groundwork for subsequent theoretical analysis and model validation.

It should be noted that all experiments in this study were conducted on artificially pressed core samples rather than on natural reservoir cores. Although artificial cores offer the advantages of controllable composition and pore structure, enabling systematic single-factor analyses, they may not fully replicate the complex diagenetic history, natural wettability, and microscopic pore-throat heterogeneity of natural reservoirs. Consequently, the experimental conclusions and the model established in this study are primarily applicable to reservoirs with pore structures and mineral compositions within the range covered

by the artificial samples. Further validation using natural core samples is necessary before extending the model to other reservoir types.

3. Experimental Results

Following the experimental measurement procedure described above, this study systematically obtained the key petrophysical parameters of the various artificial core samples that were designed and fabricated. These parameters primarily include porosity and permeability of the rocks, irreducible water saturation, and residual oil saturation—which characterize fluid occurrence features—as well as mineral compositional parameters, namely shale content and conductive mineral content. The measured basic parameter values for each core sample are presented in Table 1 below.

Table 1. Measured experimental parameters of core samples.

Group	Sample No.	Core Length	Porosity	Permeability	S_{wi}	S_{or}	ρ_0	Shale Content	Conductive Mineral Content
		(cm)	(%)	(mD)	(%)	(%)	(Ω·m)	(%)	(%)
SH1	SH1-1	4.07	24.03	64.72	29.60	29.30	13.58	4.4	/
	SH1-2	3.76	20.81	40.56	31.00	29.10	13.01	9	/
	SH1-3	3.85	19.52	35.70	33.50	28.90	12.18	13.7	/
SH2	SH2-1	3.53	24.32	82.41	30.90	30.10	11.53	3.8	6.29
	SH2-2	3.82	23.63	41.17	33.60	30.20	11.31	8.3	6.13
	SH2-3	4.11	24.06	24.78	35.10	29.60	10.67	12.7	6.50
SH3	SH3-1	4.06	26.83	69.09	32.30	30.40	11.23	3.8	13.87
	SH3-2	3.75	25.43	40.39	33.90	31.50	10.75	8.2	12.48
	SH3-3	3.91	26.31	26.65	35.40	31.60	9.49	12.1	11.33
SH4	SH4-1	3.87	22.03	6.43	34.40	31.20	10.40	4	74.16
	SH4-2	3.46	18.36	3.90	37.70	30.50	14.27	9	69.62
	SH4-3	3.32	20.48	5.69	43.50	28.40	13.53	13.4	63.63
SD	SD1-1	7.38	24.54	141.01	30.90	27.30	15.13	/	/
	SD1-2	4.68	26.90	462.95	27.50	29.70	11.83	/	/
	SD1-3	6.00	28.62	712.59	25.80	30.80	10.39	/	/
	SD1-4	5.90	32.24	2034.32	22.5	30.1	7.93	/	/
P1	P1-1	6.92	28.46	34.15	31.30	30.50	6.86	/	68.69
	P1-2	7.43	32.31	40.05	29.60	32.50	7.17	/	68.04
	P1-3	7.58	28.76	41.55	30.10	32.30	6.96	/	68.61
	P1-4	6.70	30.37	66.38	29.40	31.80	6.66	/	69.22
	P1-5	7.55	30.10	74.36	29.10	30.80	7.93	/	68.05
	P1-6	7.64	32.30	80.03	29.70	32.20	8.26	/	70.90
	P1-7	6.73	34.08	92.95	28.60	29.80	7.65	/	67.59
P2	P2-1	7.69	23.89	114.94	31.80	27.80	13.38	/	7.10
	P2-2	7.58	27.47	115.22	32.10	26.40	12.01	/	12.83
	P2-3	7.68	27.90	107.55	31.10	28.00	11.37	/	17.12
	P2-4	6.80	25.66	100.30	32.60	27.60	10.60	/	20.30
	P2-5	7.75	26.61	97.49	31.50	29.10	9.59	/	23.16

In addition, simultaneous measurements of oil–water relative permeability and resistivity were completed for each core sample under two different formation water salinity displacement conditions. All experiments were conducted at a constant temperature of 25 °C. The injection water used in the displacement experiments was Na_2CO_3 solution, with salinities set to 7000 ppm and 3000 ppm, corresponding to resistivities of 1.06 Ω·m and 2.28 Ω·m, respectively, at 25 °C. Taking core sample SH1-1 as an example, Table 2 lists the simultaneous relative permeability–resistivity measurement data for this sample under conditions of original formation water salinity of 7000 ppm and injected water salinity of 3000 ppm. The above experimental data and core parameters lay a solid data foundation for subsequent systematic studies on the experimental laws of oil–water relative permeability,

and also provide reliable data support for the establishment and accuracy validation of the relative permeability–resistivity relationship model.

Table 2. Joint measurement data of relative permeability and resistivity for sample SH1-1.

Sample No.	S_{wi} (fraction)	ρ_t (Ω·m)	Water Relative Permeability (fraction)	Oil Relative Permeability (fraction)
SH1-1	0.28	149.3	0.000	1.000
	0.33	128.7	0.004	0.817
	0.36	114.7	0.007	0.679
	0.43	93.6	0.015	0.433
	0.56	70.1	0.056	0.197
	0.64	57.4	0.099	0.081
	0.67	54.2	0.129	0.044
	0.71	51.1	0.188	0.000

4. Discussion

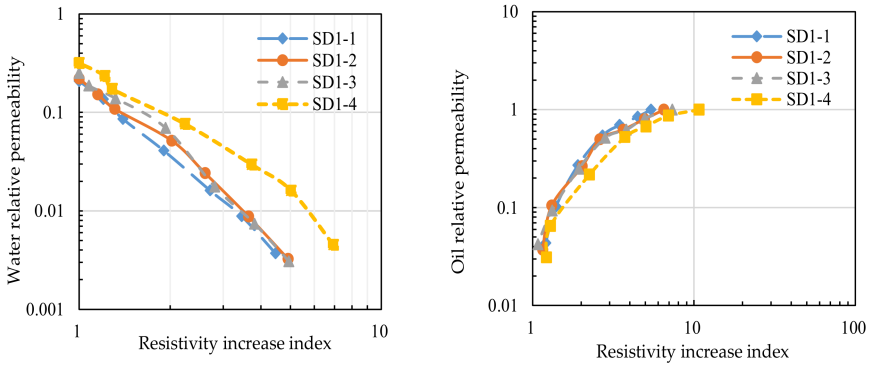
Based on the data obtained from the simultaneous measurement experiments of oil–water relative permeability and resistivity, this study adopts the control-variable method to analyze, one by one, the effects of variations in each single parameter on the co-measurement results. This approach effectively decouples the interference among multiple factors and clarifies the respective roles of these factors in seepage characteristics and electrical responses. On this basis, cross-plots are constructed to illustrate the relationships between two-phase relative permeability, resistivity index, and water saturation. The influencing mechanisms of key factors—including pore structure characteristics, conductive mineral content, shale content, and injected water salinity—on oil–water seepage behavior and resistivity response are systematically investigated. This work provides experimental evidence and theoretical support for establishing the intrinsic correlation between relative permeability and resistivity.

4.1. Effect of Pore Structure

To investigate the influence of pore structure characteristics on the relationship between seepage and electrical properties, this study selects four pure sandstone core samples from Group SD in Table 1 as the analysis subjects. These samples contain no conductive minerals or dispersed clay, yet exhibit distinctly different pore structure characteristics, with porosity ranging from 24% to 32% and permeability varying between 141 mD and 2034 mD, showing a positive correlation with porosity. Based on the simultaneous measurement data of relative permeability and resistivity for this group of samples, the influence of differences in porosity–permeability conditions on the intrinsic relationship between oil–water relative permeability and resistivity index can be independently analyzed, free from the interference of conductive minerals and clay.

Figure 4 presents the relative permeability–resistivity relationship curves for the Group SD pure sandstone samples under freshwater displacement conditions (initial water salinity 7000 ppm, injected water salinity 3000 ppm), where (a) and (b) correspond to the relationships between water relative permeability (K_{rw}) and oil-phase relative permeability (K_{ro}) with resistivity index (I), respectively. Analysis of Figure 4a reveals that, for a single core sample, K_{rw} exhibits a negative correlation with I; that is, as K_{rw} increases, I decreases progressively. Comparing across the entire group, for a given I, K_{rw} increases with improving pore-permeability conditions of the sample, indicating a positive correlation between pore structure characteristics and K_{rw}. As shown in Figure 4b, K_{ro} is positively correlated with I, meaning that a decrease in K_{ro} is accompanied by a reduction in I. Conversely,

comparing across the group, for the same I, K_{ro} tends to decrease as pore-permeability conditions improve, demonstrating a negative correlation between the comprehensive porosity-permeability condition and K_{ro}.



(**a**) k_{rw} vs. I (**b**) k_{ro} vs. I

Figure 4. Cross-plots of oil–water relative permeability and resistivity increase index for SD group pure sandstone samples.

In summary, under identical resistivity index conditions, the core pore-permeability condition is positively correlated with water relative permeability and negatively correlated with oil relative permeability.

4.2. Effect of Conductive Minerals

To clarify the influence of conductive mineral content on the relationship between water saturation and resistivity index, this study selects six core samples (SD1-1, P2-1, P2-2, P2-3, P2-4, and P2-5) for analysis. This group exhibits relatively small variations in porosity and permeability, thereby minimizing interference from the comprehensive porosity-permeability condition. In addition, all samples have zero dispersed clay content, eliminating the influence of shale content. The conductive mineral content of the six samples increases sequentially from 0% to 23% (Table 1), forming a single-variable gradient. Based on the simultaneous measurement data of relative permeability and resistivity for this sample set, the influence of varying conductive mineral content on the relationship curves between water saturation and resistivity index, as well as between relative permeability and resistivity index, can be independently analyzed.

Figure 5 illustrates the relationship between water saturation (S_w) and resistivity index (I) for core samples with different conductive mineral contents. For a single core sample, I decreases with increasing S_w, exhibiting a negative correlation. Comparing different samples, for a given S_w, I decreases as conductive mineral content increases. Further analysis reveals that at higher S_w values, the differences in I among samples are relatively small; however, at lower S_w values, these differences become substantially larger. These results indicate that conductive mineral content exerts a significant influence on the I-S_w relationship, and this effect is particularly pronounced in the low-water-saturation range.

Figure 6a illustrates the relationship between water relative permeability (*Krw*) and resistivity index (I) under varying conductive mineral contents. At the initial displacement stage with low *Krw*, I increases significantly as the conductive mineral content decreases, accompanied by large inter-sample differences; these differences gradually diminish with increasing *Krw* during displacement. At a given I, *Krw* decreases notably with higher conductive mineral content. Figure 6b presents the relationship between oil relative permeability (*Kro*) and I for different conductive mineral contents, revealing notable variations in the I–*Kro* curves among samples. At a given I, *Kro* increases with rising conductive mineral

content, indicating a positive correlation, and this positive effect weakens as I decreases (i.e., with increasing water saturation).

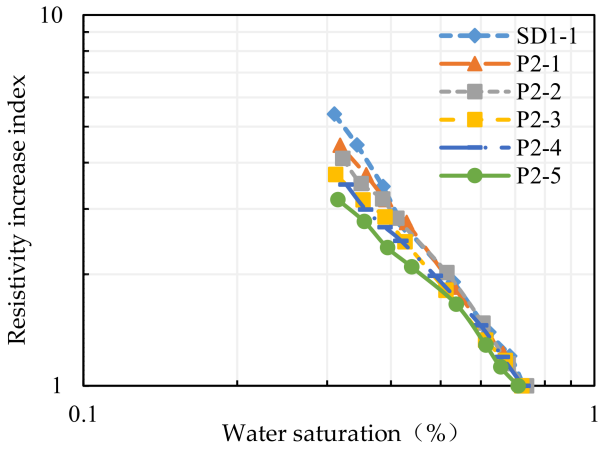
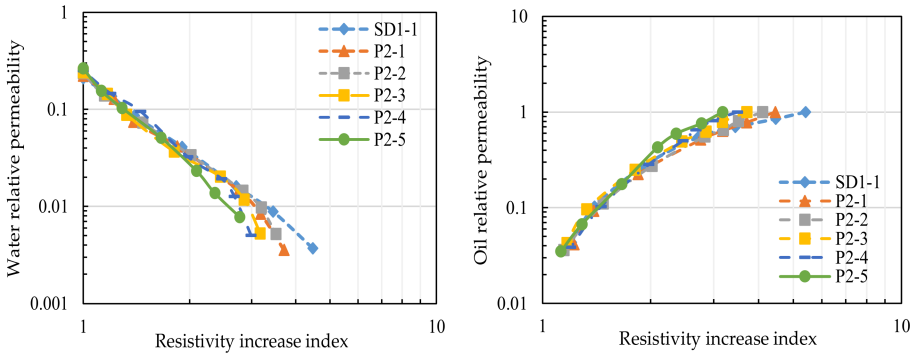


Figure 5. Cross-plot of resistivity increase index versus water saturation for rock samples with different conductive mineral contents.



(**a**) k_{rw} vs. I (**b**) k_{ro} vs. I

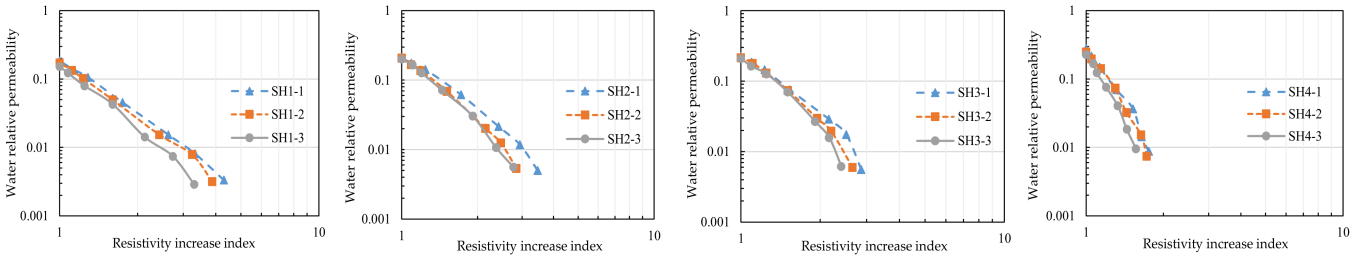
Figure 6. Cross-plot of oil–water relative permeability and resistivity increase index for rock samples with different conductive mineral contents.

4.3. Effect of Dispersed Clays

To investigate the influence of dispersed clay content on oil–water two-phase relative permeability, this study conducts parallel comparative experiments using four groups of core samples: SH1, SH2, SH3, and SH4. As shown in Table 1, the comprehensive porosity-permeability conditions of these four groups exhibit only minor differences, effectively eliminating the interference of pore structure on the experimental results. The four groups are set with different gradients of conductive mineral content: the SH1 group contains no conductive minerals; the SH2 group has a similar conductive mineral content of approximately 6%; the SH3 group has about 12%; and the SH4 group has about 70%. Within each group, the clay content of the individual core samples increases successively (specific values are given in Table 1). Figure 7a–d present cross-plots of K_{rw} versus I for the SH1–SH4 groups, respectively, and Figure 8 shows cross-plots of K_{rw} versus K_{rw} for all samples.

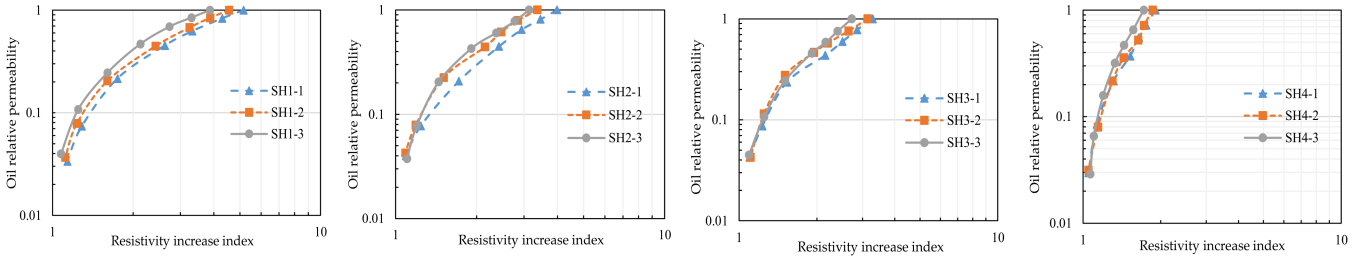
Analysis of Figure 7 reveals that from (a) to (d), the conductive mineral content of the four groups increases sequentially (0%, 6%, 12%, 70%). Comparing the figures, as the conductive mineral content rises, the right endpoints of the cross-plot curves shift leftward overall, indicating that as K_{rw} approaches zero, I decreases with increasing conductive mineral content. Within each group, for a given I, K_{rw} tends to decrease with increasing clay content. In summary, clay content is negatively correlated with K_{rw} As shown in Figure 8, with increasing conductive mineral content, the right endpoints of the cross-

plots also exhibit a general leftward shift, meaning that as K_{rw} approaches 1, I decreases with increasing conductive mineral content. Within each group, for the same I, K_{rw} tends to increase with increasing clay content. Therefore, clay content is positively correlated with K_{rw}.



(**a**) k_{rw} vs. I for SH1 group (**b**) k_{rw} vs. I for SH2 group (**c**) k_{rw} vs. I for SH3 group (**d**) k_{rw} vs. I for SH4 group

Figure 7. Cross-plot of water relative permeability and resistivity increase index for rock samples with different clay contents.



(**a**) k_{ro} vs. I for SH1 group (**b**) k_{ro} vs. I for SH2 group (**c**) k_{ro} vs. I for SH3 group (**d**) k_{ro} vs. I for SH4 group

Figure 8. Cross-plot of oil relative permeability and resistivity increase index for rock samples with different clay contents.

4.4. Effect of Brine Salinity

To simulate the influence of formation water salinity variations on reservoir seepage and electrical conductivity characteristics during oilfield development, two sets of comparative displacement experiments were designed as described above. First, simultaneous relative permeability–resistivity measurements were conducted under conditions where both the initial saturation water and injected water had a salinity of 7000 ppm. Subsequently, while keeping all other conditions unchanged, the injected water salinity was reduced to 3000 ppm, and the experimental procedure was repeated to simulate the common freshwater flooding process encountered in oilfield production. Two pure sandstone core samples, SD1-1 and SD1-4, with significantly different porosity-permeability conditions (ensuring zero conductive mineral and clay content to eliminate their interference in the analysis), were selected to construct cross-plots of water saturation versus resistivity under the two injected water salinities, as shown in Figure 9. Analysis indicates that at the same S_w, higher injected water salinity corresponds to lower rock resistivity; moreover, as S_w increases, the difference in resistivity for the same sample under different salinity conditions becomes progressively larger. This demonstrates that the resistivity reduction effect is more pronounced under high-salinity water displacement conditions.

Figure 10a,b present cross-plots of relative permeability versus I for core samples SD1-1 and SD1-4 under injected water salinities of 7000 ppm and 3000 ppm, respectively. From the cross-plot of K_{rw} versus I shown in Figure 10a, it can be observed that for a given I, a higher injected water salinity corresponds to a larger K_{rw}. Moreover, this difference increases with the improvement in the sample's porosity-permeability condition, meaning that the separation of K_{rw} at different salinities is more pronounced for sample

SD1-4, which has better pore-permeability conditions. From the cross-plot of K_{ro} versus I shown in Figure 10b, it is evident that for the same I, K_{ro} decreases with increasing injected water salinity. Additionally, as the porosity-permeability condition improves, this decreasing trend becomes more obvious. In summary, under the same I condition, injected water salinity is positively correlated with K_{rw} and negatively correlated with K_{ro}; furthermore, both of these correlation effects are enhanced with the improvement in the sample's porosity-permeability condition.

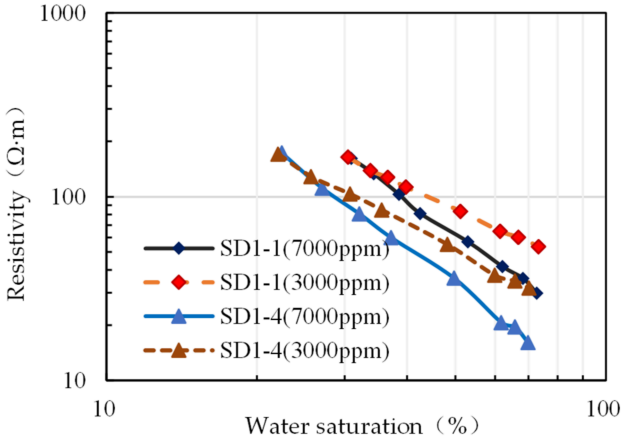
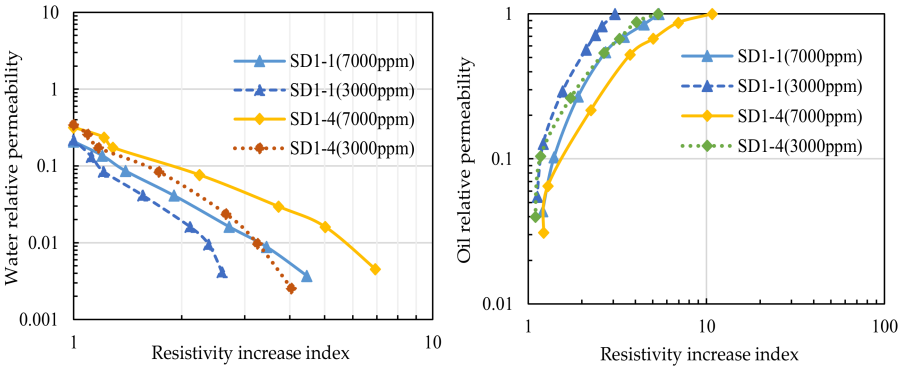


Figure 9. Cross-plot of water saturation versus resistivity under varying brine salinity conditions.



(**a**) k_{rw} vs. I (**b**) k_{ro} vs. I

Figure 10. Cross-plot of oil–water relative permeability and resistivity increase index for rock samples under different brine salinity displacement conditions.

5. Theoretical Simulation

Based on the experimental analyses of multiple groups of core samples described above, it is demonstrated that pore structure and mineral composition exert significant influences on the electrical conductivity and relative permeability characteristics of rocks. To address this, the study first focuses on pure sandstone formations. By leveraging the geometric similarity between the conductive path of movable water and the seepage path, and combining seepage theory with electrical conduction theory, a relative permeability–resistivity relationship equation is derived and established for pure sandstone, which is equivalent to conduction solely by movable water. Subsequently, considering the complexity of actual reservoirs, the generalized Archie equation—capable of characterizing the electrical conductivity of multi-component rocks—is further introduced to correct for the effects of variations in conductive mineral and shale content on rock conductivity. Integrating the above theoretical developments, this study ultimately establishes an oil–water relative permeability–resistivity relationship model applicable to complex argillaceous sandstone reservoirs containing conductive minerals. The validity and accuracy of the

model are verified using measured data, and the overall derivation workflow is illustrated in Figure 11.

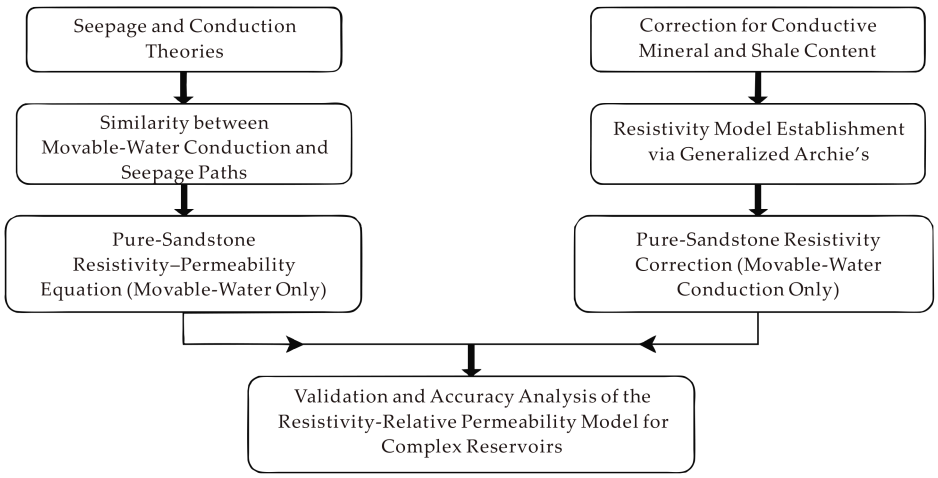


Figure 11. Schematic diagram of the model derivation procedure.

5.1. Modeling

Although the model established in previous studies can effectively characterize the effects of complex pore structures and argillaceous conductivity on the relative permeability–resistivity relationship, the inherent differences between seepage and conductive conditions in complex argillaceous sandstone reservoirs containing conductive minerals may compromise its prediction accuracy when applied directly. Therefore, in the theoretical model construction of this study, the comprehensive influences of multiple components—including pore structure, shale content, and conductive minerals—on rock conductivity and relative permeability characteristics are systematically taken into account. For such reservoirs, the electrical conductivity arises from the combined contributions of conductive mineral matrix, argillaceous components, bound water, and movable water; whereas the seepage path is associated only with the flow of movable water. Based on the similarity between the conductive path of movable water and the seepage path, and by integrating seepage theory with electrical conduction theory, a relative permeability–resistivity relationship equation is derived for pure sandstone, which is equivalent to conduction solely by movable water, serving as the theoretical foundation for subsequent construction of the complex reservoir model.

To further enhance the applicability and generalizability of the model in practical reservoir interpretation, this study redefines and improves the parameter variables based on the theoretical model of Guo et al. [43]. Specifically, a saturation parameter S^*_{wf} is introduced to characterize the relative content of movable water; I_r is defined as the resistivity index of the equivalent pure sandstone (conducting only through movable water); and a fractional term is added to the water-phase relative permeability K_{rw} equation to ensure theoretical correctness under the two extreme boundary conditions of fully water-saturated and fully oil-saturated formations. The final equation of the equivalent pure sandstone relative permeability–resistivity relationship is given as follows (for detailed derivation, refer to [43]):

$$\begin{cases} K_{rw} = a \cdot I_r^{-k_1} \cdot {S^*_{wf}}^{k_2} + (1-a) \cdot I_r^{-k_3} \cdot {S^*_{wf}}^{k_4} \\ K_{ro} = b\left(1 - S^*_{wf}\right)^{n_1} \left(1 - \frac{S^*_{wf}}{I_r}\right)^{n_2} + (1-b)\left(1 - S^*_{wf}\right)^{n_3} \left(1 - \frac{S^*_{wf}}{I_r}\right)^{n_4} \\ S^*_{wf} = \frac{S_w - S_{wi}}{1 - S_{or} - S_{wi}} \end{cases} \quad (1)$$

where K_{rw} and K_{ro} denote the relative permeabilities of the water and oil phases, respectively, in fraction; I_r is the resistivity index of the equivalent pure sandstone (based on the assumption that only movable water conducts electricity), dimensionless. The undetermined coefficients in the model are divided into two groups: the water-phase relative permeability model contains five coefficients (a, k_1, k_2, k_3 and k_4); the oil-phase relative permeability model contains five parameters (b, n_1, n_2, n_3 and n_4). The introduction of these coefficients is intended to enhance the adaptability and general applicability of the model to various types of complex reservoirs. In addition, S_w is the water saturation, fraction; S_{wi} is the irreducible water saturation, fraction; S_{or} is the residual oil saturation, fraction; and S^*_{wf} is a introduced saturation parameter used to characterize the relative content of movable water.

To overcome the limitations of the previous model in describing the complexity of multi-component mineral compositions, this study further introduces the generalized Archie equation to characterize the electrical conductivity of multi-component rocks, thereby correcting for the effects of variations in conductive mineral and shale content on rock conductivity, and accordingly establishing a method for determining the resistivity index I_r of the equivalent pure sandstone. In 2010, Glover [16], addressing the limitation that the classical Archie equation is only applicable to pure sandstone formations, proposed a generalized Archie equation capable of describing the electrical conductivity of rocks containing N components. Applying this theory to the complex argillaceous sandstone reservoirs containing conductive minerals investigated in this study, the conductivity equation can be expressed as follows:

$$C_t = C_{ma}V_{ma}^{m_{ma}} + C_{sh}V_{sh}^{m_{sh}} + C_w\phi^m(S_w - S_{wi})^{m_{wf}} + C_w\phi^m S_{wi}^{m_{wi}} \quad (2)$$

where C_t is the total electrical conductivity of the rock, S/m; C_{ma}, C_{sh}, and C_w are the electrical conductivities of conductive minerals, shale, and formation water, respectively, S/m; V_{ma} and V_{sh} are the volume fractions of conductive minerals and shale, respectively, fraction; ϕ is the effective porosity of the reservoir, fraction; and m_{ma}, m_{sh}, m, m_{wf}, and m_{wi} are the conductivity exponents of conductive minerals, shale, pore fluid, movable water, and bound water, respectively, dimensionless.

From the theoretical analysis of Equation (2) above, it can be seen that the generalized Archie equation not only provides a unified description of the complex electrical conductivity of rocks under the combined effects of conductive minerals, shale, and formation water, but also features a concise mathematical form that facilitates the determination and application of reservoir parameters such as water saturation in practical production. Based on this conductivity theory, this study further employs the equation to correct for the conductive contributions of conductive minerals, shale, and bound water in the reservoir, and derives the following formula for calculating the conductivity of the equivalent pure sandstone that conducts electricity solely through movable water:

$$C'_t = C_t - C_w\phi^m S_{wi}^{m_{wi}} - C_{sh}V_{sh}^{m_{sh}} - C_{ma}V_{ma}^{m_{ma}} \quad (3)$$

where C'_t is the corrected electrical conductivity of the equivalent pure sandstone that conducts electricity solely through movable water, S/m.

As analyzed above, to obtain the resistivity index I_r of the equivalent pure sandstone in the relative permeability–resistivity model, it is first necessary to determine the equivalent conductivity of the rock under fully water-saturated conditions. According to the definition of the resistivity index, this conductivity should exclude the contributions of non-movable-water conductive components, such as conductive minerals, shale, and bound water. To this end, based on the theoretical framework of the generalized Archie equation presented

above, a step-by-step correction of the aforementioned components is performed, yielding the corrected conductivity of the water-saturated rock as follows:

$$C_o' = C_o - C_w\phi^m S_{wi}^{m_{wi}} - C_{sh}V_{sh}^{m_{sh}} - C_{ma}V_{ma}^{m_{ma}} \quad (4)$$

where C_o' is the corrected electrical conductivity of the equivalent water-saturated pure sandstone that conducts electricity solely through movable water, S/m.

According to the definition of the resistivity index, $I_r = \boldsymbol{\rho_t}/\boldsymbol{\rho_o} = C_o'/C_t'$. By combining Equations (3) and (4), the expression for the resistivity index I_r of the equivalent pure sandstone that conducts electricity solely through movable water can be determined as follows:

$$I_r = \frac{C_o - C_{wi}\phi^m S_{wi}^{m_{wi}} - C_{sh}V_{sh}^{m_{sh}} - C_{ma}V_{ma}^{m_{ma}}}{C_t - C_{wi}\phi^m S_{wi}^{m_{wi}} - C_{sh}V_{sh}^{m_{sh}} - C_{ma}V_{ma}^{m_{ma}}} \quad (5)$$

To simplify the expression of the above formula, a correction quantity C^* is now introduced, defined as follows:

$$C^* = C_w\phi^m S_{wi}^{n_{wi}} + C_{sh}V_{sh}^{m_{sh}} + C_{ma}V_{ma}^{m_{ma}} \quad (6)$$

Using the definition of the correction quantity C^*, Equation (5) can be simplified as follows:

$$I_r = \frac{C_o - C^*}{C_t - C^*} \quad (7)$$

Based on the above theoretical analysis, by combining the corrected expression of the resistivity index for the equivalent pure sandstone with the relative permeability calculation formula (Equation (1)), this study ultimately establishes an oil–water relative permeability and resistivity relationship model applicable to complex argillaceous sandstone reservoirs containing conductive minerals, with the expression given as follows:

$$\begin{cases} K_{rw} = a \cdot \left(\frac{C_t - C^*}{C_o - C^*}\right)^{k_1} \cdot \left(\frac{S_w - S_{wi}}{1 - S_{or} - S_{wi}}\right)^{k_2} + (1-a) \cdot \left(\frac{C_t - C^*}{C_o - C^*}\right)^{k_3} \cdot \left(\frac{S_w - S_{wi}}{1 - S_{or} - S_{wi}}\right)^{k_4} \\ K_{ro} = b\left(1 - \left(\frac{S_w - S_{wi}}{1 - S_{or} - S_{wi}}\right)\right)^{n_1}\left(1 - \left(\frac{S_w - S_{wi}}{1 - S_{or} - S_{wi}}\right)\left(\frac{C_t - C^*}{C_o - C^*}\right)\right)^{n_2} \\ \quad +(1-b)\left(1 - \left(\frac{S_w - S_{wi}}{1 - S_{or} - S_{wi}}\right)\right)^{n_3}\left(1 - \left(\frac{S_w - S_{wi}}{1 - S_{or} - S_{wi}}\right)\left(\frac{C_t - C^*}{C_o - C^*}\right)\right)^{n_4} \end{cases} \quad (8)$$

The coefficients and exponents incorporated in the final model are all derived through rigorous simplification during the derivation process outlined above, and they possess clear physical meanings that effectively characterize the intrinsic relationship between relative permeability and resistivity. The introduction of these parameters not only ensures the theoretical rigor of the model but also significantly enhances its prediction accuracy and application value in practical oilfield development.

5.2. Experimental Verification

To verify the correctness and applicability of the model established in this study, multiple sets of core experimental data measured in the previous sections are employed for experimental validation and accuracy analysis. Six core samples with the most complex mineral compositions among the conductive-mineral-bearing argillaceous sandstone samples (SH2 and SH3 groups) are selected. Based on the proposed resistivity model and correction method, the resistivity index I_r of the equivalent pure sandstone that conducts electricity solely through movable water is determined for each sample. Using the experimental resistivity data, a Newton–Raphson iterative algorithm coded in C language is applied to optimally solve for the five conductivity exponents (m_{ma}, m_{sh}, m, m_{wf}, m_{wi}) in the generalized Archie equation (Equation (2)). The objective function of the optimization algorithm is defined as the sum of

squared relative residuals between the calculated conductivity (derived from Equation (2)) and the measured conductivity. The convergence criterion for the iteration was set as the relative change in the objective function between two consecutive iterations, with convergence deemed achieved when $|F(x_\{k + 1\}) - F(x_k)| / |F(x_k)| < 1.0 \times 10^{-10}$. In addition, a maximum of 200 iterations was specified as a safeguard against non-convergence. Based on classical petrophysical theory, the typical values of the relevant indices are generally close to 2.0. Consequently, each of the five unknown parameters to be determined is constrained within a physically reasonable interval of [0.5, 3.0], with the initial guess set to 2.0—the center of this feasible region—to effectively avoid boundary violations during iteration. Through the aforementioned optimization algorithm, the optimal set of the five parameters for each core sample is successfully obtained.

Subsequently, the response relationships between the optimized parameters and multiple petrophysical parameters—including pore structure parameters and mineral component contents—are analyzed, and the optimal calculation relationships between the five unknown parameters and the reservoir parameters of the core samples are established and selected. The correlation analysis results (Figure 12) indicate that the conductivity exponent m_{ma} exhibits the best correlation with irreducible water saturation S_{wi}; the shale conductivity exponent m_{sh} shows the best correlation with the volume fraction of shale V_{sh}; the pore-fluid conductivity exponent m is best correlated with porosity; the movable-water conductivity exponent m_{wf} remains relatively stable, with values concentrated around 0.814 for all samples; and the bound-water conductivity exponent m_w shows the best correlation with residual oil saturation S_{or}. These regression analysis results further validate the theoretical rationality of the physical meanings assigned to each parameter in the proposed model. Based on the above optimization results, the calculation relationships between the undetermined coefficients of the resistivity model and the reservoir parameters are established as follows:

$$\begin{cases} m_{ma} = -0.0918 S_{wi} + 4.2133 \\ m_{sh} = -0.075 V_{sh} + 1.8033 \\ m = 0.064\phi + 0.835 \\ m_{wf} = 0.814 \\ m_{wi} = -0.0707 S_{or} + 3.1257 \end{cases} \quad (9)$$

The goodness-of-fit statistics for the regression equations (Equation (9)) are as follows: the coefficient of determination R^2 values are 0.639 for m_{ma} vs. S_{wi}, 0.938 for m_{sh} vs. V_{sh}, 0.95 for m vs. porosity, and 0.771 for m_{wi} vs. S_{or}. In contrast, m_{wf} remained nearly constant across all samples and was therefore treated as a fixed value (0.814) rather than as a regression variable. Among these correlations, the coefficient of determination for the m_{ma} vs. S_{wi} relationship (R^2 = 0.639) is lower than those of the other exponent–parameter relationships. This is because mma characterizes the conductive efficiency of the conductive-mineral network, which depends not only on the volumetric fraction of conductive minerals (indirectly reflected by Swi, since higher conductive-mineral content reduces effective pore space and increases irreducible water saturation) but also on the spatial connectivity and particle–particle contact geometry of the conductive phase—features that vary even among samples with similar bulk compositions. Nevertheless, multiple rounds of model validation demonstrate that the model yields high prediction accuracy, with all calculated parameters falling within the acceptable error range.

Using the equivalent pure sandstone resistivity index I_r determined above, combined with the simultaneous measurement data of relative permeability and resistivity for the selected core samples, an optimization calculation is performed under constraint conditions to determine the unknown parameters in the relative permeability–resistivity relationship model established in this study. Subsequently, the variation patterns of the model param-

eters across different core samples are analyzed comparatively, and optimal calculation relationships between these parameters and reservoir petrophysical properties are established and selected. Finally, the optimized parameters are substituted into the relative permeability–resistivity model, and the model accuracy is evaluated by comparing the calculated relative permeability values with experimental measurements, thereby verifying its correctness and analyzing its practical application performance.

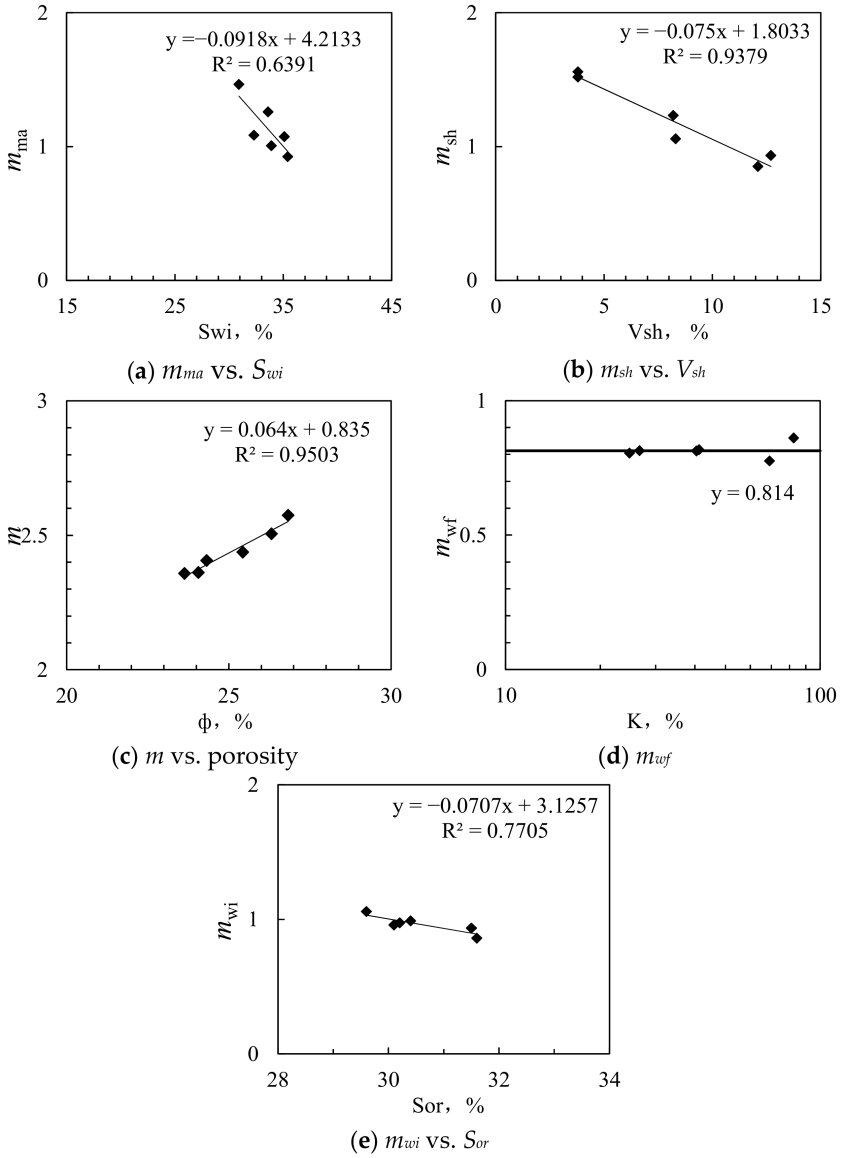


Figure 12. Cross-plots of the resistivity equation coefficients against reservoir parameters.

Based on the final oil–water relative permeability–resistivity relationship model equation (Equation (8)), the optimization technique is first employed to perform constrained optimization calculations on the water-phase relative permeability experimental data, yielding the five undetermined parameters (a, k_1, k_2, k_3, k_4) in the water-phase relative permeability model for each core sample. Following the same methodology used for establishing and selecting the calculation relationships for the undetermined coefficients of the resistivity model described above, the response relationships between the optimized parameters and petrophysical properties, pore structure parameters, mineral contents, etc., are analyzed. The optimal calculation relationships between the undetermined coefficients in the water-phase relative permeability model and the reservoir parameters are then established and selected as presented in Equation (10). The goodness-of-fit of these regres-

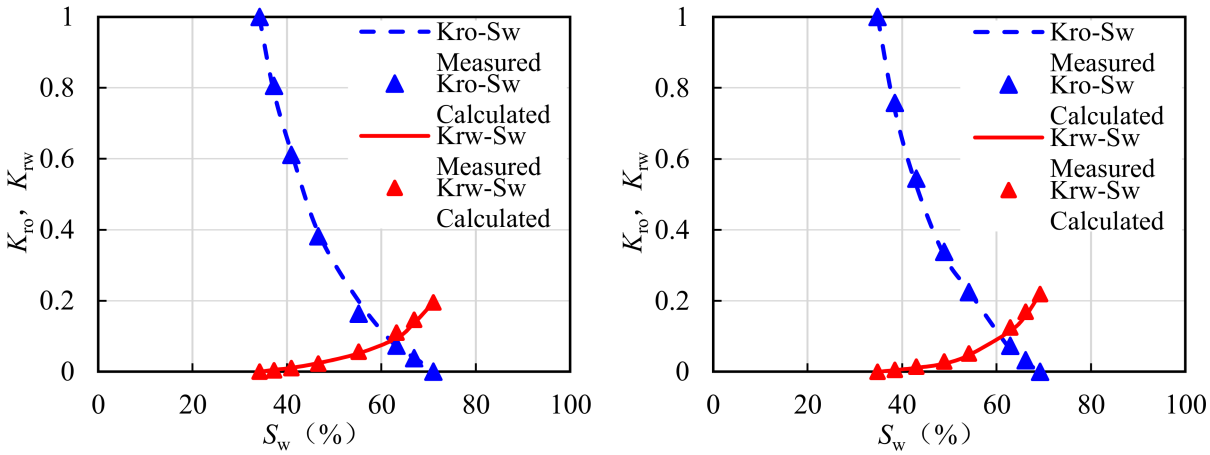
sion equations, evaluated by the coefficient of determination R^2, yields values ranging from 0.61 to 0.97, reflecting an acceptable to excellent level of predictive capability for the derived correlations.

$$\begin{cases} a = 0.0964V_{ma} - 0.3282 \\ k_1 = -0.3503S_{wi} + 12.271 \\ k_2 = 1.2389S_{or} - 35.533 \\ k_3 = 0.2885S_{or} - 8.5827 \\ k_4 = -1.1118\phi + 29.845 \end{cases} \quad (10)$$

Similarly, based on the simultaneous measurement data of oil-phase relative permeability and resistivity, the same constrained optimization algorithm is employed to obtain the five undetermined parameters (b, n_1, n_2, n_3 and n_4) in the oil-phase relative permeability model for each core sample. By analyzing the characteristic patterns of the optimized parameters for each sample, the optimal calculation relationships between the undetermined coefficients in the oil-phase relative permeability model and the reservoir parameters are established and selected in Equation (11). The goodness-of-fit for the oil-phase regression equations yields R^2 values ranging from 0.613 to 0.782.

$$\begin{cases} b = 0.1637V_{ma} + 3.1174 \\ n_1 = -0.1168\rho_o + 2.3188 \\ n_2 = -0.0179S_{wi} + 1.1189 \\ n_3 = -0.1634\rho_o + 2.3967 \\ n_4 = 0.0036K + 0.8939 \end{cases} \quad (11)$$

Using the calculation relationships established above, the parameter values in the relative permeability–resistivity relationship model are determined for each core sample and then substituted into the model to obtain the calculated relative permeability values. Based on the model derivation process presented in Section 5.1, the SH2 and SH3 groups exhibit the most complex compositions among all samples and involve the largest number of parameters under the applicable conditions of the proposed model (as listed in Table 1). The remaining sample groups possess relatively simpler compositions, i.e., some parameters have zero values during model calculation, which reduces the difficulty of coefficient determination to a certain extent. Therefore, the SH2 and SH3 groups, characterized by the most complex rock compositions capable of fully validating the applicability of the proposed model, were selected for the final model validation. The results show that the errors for water-phase relative permeability range from 3.0% to 8.8%, and those for oil-phase relative permeability range from 2.0% to 13.4%, further confirming that the validation errors in this study are representative rather than coincidental. Figure 13 presents the comparison between model-calculated and experimentally measured relative permeabilities. Specifically, for sample SH2-3, the average relative errors for water-phase and oil-phase relative permeabilities are 9.8% and 4.4%, respectively; for sample SH3-3, the corresponding values are 13.4% and 5.4%. Theoretical analysis and accuracy comparison across multiple core samples demonstrate that the model-calculated values are in good agreement with the measured data, validating the high calculation accuracy of the proposed model. This model effectively characterizes the two-phase seepage behavior in complex argillaceous sandstone reservoirs containing conductive minerals, significantly improving the calculation accuracy of oil–water relative permeability, and provides a new theoretical foundation and technical approach for accurately predicting relative permeability using electrical parameters.



(**a**) Measured vs. calculated for SH2-3 (**b**) Measured vs. calculated for SH3-3

Figure 13. Comparison of model-calculated relative permeability with measurements.

It should be noted that the proposed model is not universally applicable to all reservoir types. Its effective application presupposes that the pore-throat structure characteristics of the pore space within the target interval remain approximately constant or vary only within a predictable range. Once the pore structure undergoes dramatic changes, the geometric similarity between the conductive pathways (governed by movable water distribution) and the seepage pathways—which serves as the theoretical foundation of the model—will be significantly weakened. Furthermore, the regression relationships between the model coefficients and reservoir parameters (Equations (9)–(11)) are established based on the porosity–permeability characteristics of the artificial core samples used in this study. When extending the model to reservoirs with distinctly different pore structure characteristics, recalibration of the relevant coefficients is required. For highly heterogeneous reservoirs, it is recommended that model parameters be established separately according to flow units or lithofacies types.

In practical applications, the model established in this study enables the continuous prediction of oil–water relative permeability in complex reservoirs using conventional well-logging data. The implementation procedure is outlined as follows. First, key petrophysical parameters of the reservoir are derived from the standard logging suite: porosity is computed from neutron–density or sonic logs, clay content is determined from natural gamma-ray or spectral gamma-ray logs, conductive mineral composition and its types are retrieved from elemental capture spectroscopy or induced polarization logs, and water saturation is obtained from resistivity measurements. For intervals where specialized logging data are available, nuclear magnetic resonance T_2 distribution spectra and borehole imaging logs can be further incorporated to extract pore geometry attributes, such as grain size or pore-throat radius. Upon the complete determination of the aforementioned reservoir parameters, and by integrating the resistivity–relative permeability relationship model developed in this study along with the corresponding parameter calibration methodology, the continuous-depth profiles of oil and water relative permeabilities can be computed over the target logged interval—owing to the inherently continuous sampling nature of well logs. This approach effectively overcomes the limitation of discrete core-plug measurements, which provide information only at sparse depth points.

In the study of seepage and electrical conductivity laws and the model establishment process, this paper systematically considers the comprehensive effects of factors such as pore structure, conductive minerals, shale content, and formation water salinity on rock seepage and electrical conductivity characteristics. Based on theoretical derivation and validation with measured data, a relationship model between oil–water relative permeability

and resistivity applicable to complex argillaceous sandstone reservoirs containing conductive minerals has been established. Nevertheless, certain limitations remain in the proposed model regarding microscopic mechanism characterization and complex seepage behavior representation. First, the model development and validation are primarily based on artificial core experiments, necessitating further verification using natural core samples to confirm its applicability under actual reservoir conditions. Second, the conductive mineral analysis is restricted to pyrite—the most common conductive mineral in natural reservoirs—leaving the generalizability to other conductive minerals (e.g., siderite, magnetite) open to question. Third, only two salinity levels were employed in the waterflooding experiments, which is insufficient to establish a comprehensive salinity-dependent calibration function. In future work, the experimental program will be expanded to incorporate additional controlling factors, including lithology, wettability, temperature, and overburden pressure, alongside natural core validation. Concurrently, theoretical advancements will pursue non-Darcy flow mechanisms, complex conductivity dispersion, and digital rock-based auxiliary calibration techniques to enhance both the physical rigor and predictive accuracy of the model.

6. Conclusions

(1) Through systematic artificial core sample fabrication and experimental procedure design, this study obtained multiple key parameters covering reservoir petrophysical properties, fluid occurrence characteristics, and mineral compositions, thereby establishing a relatively comprehensive experimental data system of simultaneous relative permeability–resistivity measurements under various porosity-permeability structures, mineral compositions, and salinity conditions. This experimental scheme provides reliable data support and constraint conditions for revealing the influencing mechanisms between relative permeability and resistivity, as well as for subsequent theoretical modeling and model validation.

(2) Using the control-variable method, the influences of pore structure, conductive mineral content, shale content, and formation water salinity on the relative permeability–resistivity relationship were systematically analyzed. The results indicate that the suppressing effect of increasing conductive-mineral content on the resistivity index is significantly enhanced at low water saturations, whereas the influence of injected-water salinity becomes more prominent at high water saturations. Under the same resistivity index condition, both conductive mineral content and shale content are negatively correlated with water-phase relative permeability and positively correlated with oil-phase relative permeability. In contrast, core porosity-permeability conditions and injected water salinity are positively correlated with water-phase relative permeability and negatively correlated with oil-phase relative permeability. Moreover, the effect of salinity on the relative permeability–resistivity relationship is enhanced as the porosity-permeability condition improves.

(3) Based on the geometric similarity between the movable-water conductive path and the seepage path, and by integrating seepage theory with conductivity equations, this study derived a relative permeability–resistivity relationship equation for equivalent pure sandstone that conducts electricity solely through movable water. By introducing the generalized Archie equation to correct for the effects of conductive mineral and shale content on rock conductivity, an oil–water relative permeability–resistivity relationship model applicable to complex argillaceous sandstone reservoirs containing conductive minerals was ultimately established. The parameters in the model have clear physical meanings and effectively characterize the intrinsic relationship between relative permeability and resistivity.

(4) The Newton–Raphson iterative algorithm was employed to optimally solve for the model parameters, and calculation relationships between the undetermined coefficients

and reservoir parameters were established. Using the two core samples with the most complex mineral compositions as validation examples, the average relative errors of the model-calculated water-phase relative permeability are 9.8% and 13.4%, while those for oil-phase relative permeability are 4.4% and 5.4%, respectively, indicating high prediction accuracy of the model. This model provides a new theoretical basis and technical approach for predicting relative permeability in complex reservoirs using electrical parameters. While the proposed model demonstrates satisfactory performance on artificial core experiments, its limitations concerning natural core validation, generalizability to diverse conductive minerals, and systematic salinity effects remain to be addressed. Future work will incorporate additional experimental variables (lithology, wettability, temperature, and overburden pressure) alongside natural core verification, and explore theoretical improvements incorporating non-Darcy flow, complex conductivity dispersion, and digital rock-based calibration to further enhance model applicability and predictive accuracy.

Author Contributions: Methodology, Z.G. and Q.F.; experiments and measurements, Y.Z.; software, Z.L.; validation, Z.G., Q.F., and Y.L.; data analysis, Y.Z.; writing—original draft preparation, Z.G.; writing—review and editing, Q.F., Z.L., and Y.Z.; funding acquisition, Z.G. All authors have read and agreed to the published version of the manuscript.

Funding: This research was supported by Heilongjiang Provincial Natural Science Foundation of China, "Study on Logging Evaluation Method of Water-flooded Zones Based on Seepage and Conduction Laws" (No. LH2023D013).

Institutional Review Board Statement: Not applicable.

Informed Consent Statement: Not applicable.

Data Availability Statement: The original data used in this study are included in this article. Further inquiries can be directed to the corresponding author.

Acknowledgments: The authors acknowledge all the participants and administrators in this study.

Conflicts of Interest: Author Yuhao Li was employed by the company Daqing International Exploration and Development Company. The remaining authors declare that the research was conducted in the absence of any commercial or financial relationships that could be construed as a potential conflict of interest.

Abbreviations

The following abbreviations are used in this manuscript:

K_{rw}	Water-phase relative permeability (fraction)
K_{ro}	Oil-phase relative permeability (fraction)
I	Resistivity increase index, $\boldsymbol{\rho_t/\rho_0}$ (dimensionless)
I_r	Resistivity index of equivalent pure sandstone (dimensionless)
S_w	Water saturation (fraction)
S_{wi}	Irreducible water saturation (fraction)
S_{or}	Residual oil saturation (fraction)
S^*_{wf}	Saturation parameter characterizing relative movable-water content
ρ_t	True resistivity of rock (Ω·m)
ρ_0	Resistivity of fully water-saturated rock (Ω·m)
φ	Effective porosity (fraction)
C_t	Total electrical conductivity of rock (S/m)
C_{ma}	Electrical conductivity of conductive minerals (S/m)
C_{sh}	Electrical conductivity of shale (S/m)
C_w	Electrical conductivity of formation water (S/m)

C_t'	Corrected conductivity of equivalent pure sandstone (S/m)
C_o'	Corrected conductivity of equivalent water-saturated pure sandstone (S/m)
V_{ma}	Volume fraction of conductive minerals (fraction)
V_{sh}	Volume fraction of shale (fraction)
m	Pore-fluid cementation exponent (dimensionless)
m_{ma}	Conductive-mineral conductivity exponent (dimensionless)
m_{sh}	Shale conductivity exponent (dimensionless)
m_{wf}	Movable-water conductivity exponent (dimensionless)
m_{wi}	Bound-water conductivity exponent (dimensionless)
a, k_1–k_4	Empirical coefficients in water-phase relative permeability model (dimensionless)
b, n_1–n_4	Empirical coefficients in oil-phase relative permeability model (dimensionless)

References

1. Kobranova, V.N. *Petrophysics*; Nedra Publishers: Moscow, Russia, 1986.
2. Waxman, M.; Thomas, E. Electrical conductivities in shaly sands—I. The relation between hydrocarbon saturation and resistivity index; II. The temperature coefficient of electrical conductivity. *J. Pet. Technol.* **1974**, *26*, 213–225. [CrossRef]
3. Clavier, C.; Coates, G.; Dumanoir, J. Theoretical and experimental bases for the dual-water model for interpretation of shaly sands. *SPE J.* **1984**, *24*, 153–168. [CrossRef]
4. De Lima, O.; Sharma, M. A grain conductivity approach to shaly sandstones. *Geophysics* **1990**, *55*, 1347–1356. [CrossRef]
5. Waxman, M.; Smits, L. Electrical conductivities in shaly sands. *SPE J.* **1968**, *8*, 107–122. [CrossRef]
6. Li, K. A new method for calculating two-phase relative permeability from resistivity data in porous media. *Transp. Porous Media* **2008**, *74*, 21–33. [CrossRef]
7. Li, K.; Shapiro, M.; Horne, R.; Ma, S.; Hajari, A.; Mudhhi, M. In situ estimation of relative permeability from resistivity measurements. *Pet. Geosci.* **2014**, *20*, 279–288. [CrossRef]
8. Guo, Y.; Pan, B.; Liu, W. A research on the relationship between resistivity index and relative permeability at different measurement conditions based on the pore structure. *Environ. Fluid Mech.* **2016**, *16*, 1129–1141. [CrossRef]
9. Hu, W.; Yang, S.; Liu, G.; Wang, Z.; Wang, P.; Lei, H. A new correction method for oil–water relative permeability curve on the basis of resistivity and water saturation relationship. *Transp. Porous Media* **2015**, *109*, 385–401. [CrossRef]
10. Pei, J.; Zhang, Y.; Hu, J.; Zhang, J.; Zhu, X.; Wang, Q.; Gong, H. Experimental verification of reservoirs with different wettability using an oil-water relative permeability model. *Processes* **2022**, *10*, 1211. [CrossRef]
11. Hu, W.; Yang, S.; Zhai, Y.; Zhu, G.; Wan, M.; Wang, W. A new optimization and correction method of oil-water phase relative permeability curve. *Acta Pet. Sin.* **2014**, *35*, 740–746.
12. Alusta, G.; Sbiga, H. Relative permeability predicted using resistivity index and capillary pressure data. *ARPN J. Eng. Appl. Sci.* **2019**, *14*, 3745–3753.
13. Xie, W.; Yin, Q.; Guan, W.; Wang, G.; Lai, J. Estimating the relative permeability from the electrical parameters of sandstone with a complex pore structure. *Energy Fuels* **2020**, *34*, 14287–14298. [CrossRef]
14. Zhang, H.; Zhao, B.; Dong, S.; Wang, X.; Jing, P. A method for the inversion of reservoir effective permeability based on time-lapse resistivity logging data and its application. *Geofluids* **2022**, *2022*, 8704344. [CrossRef]
15. Koelman, J.M.V.A.; de Kuijper, A. An effective medium model for the electric conductivity of an N-component anisotropic and percolating mixture. *Phys. A* **1997**, *247*, 10–22. [CrossRef]
16. Glover, P. A generalized Archie's law for n phases. *Geophysics* **2010**, *75*, E247–E265. [CrossRef]
17. Han, T.; Clennell, M.B.; Pervukhina, M. Modelling the low-frequency electrical properties of pyrite-bearing reservoir sandstones. *Mar. Pet. Geol.* **2016**, *78*, 549–559. [CrossRef]
18. Ohta, Y.; Mogi, T.; Ichihara, H.; Yamaoka, K.; Adachi, M.; Kubo, T.; Natsume, I. Subsurface resistivity and sulfide filling microfractures: A rock physical analysis at Mt. Ontake volcano's southeast flank. *Geophys. J. Int.* **2025**, *241*, 1448–1463. [CrossRef]
19. Janishevskii, A.; Ten, T.; Ezhova, A. Pyritization effect on well logging parameters in Jurassic reservoirs within S-E Western Siberian oil fields. *Earth Environ. Sci.* **2021**, *720*, 012098.
20. Mu, L. Investigation on mechanism of low-resistivity formation of A Oilfield. *Acta Pet. Sin.* **2005**, *21*, 189–194.
21. Miao, X.; Lu, W.; Yu, Y.; Liu, X.; Zhan, H.; Zhao, K. Tunable resistive switching in shales. *Results Phys.* **2022**, *38*, 105619. [CrossRef]
22. Shi, Y.; Meng, H.; Liu, T.; Zhang, H.; Wang, C. Evaluation of relative permeability from resistivity data for fractal porous media. *Petrophysics* **2020**, *61*, 298–310. [CrossRef]
23. Wei, W.; Hu, X.; Cai, H.; Cai, J.; Glover, P.W.J.; Lorinczi, P.; Han, Q. A fractal interpretation of Archie-like equation for partially saturated porous media. *Water Resour. Res.* **2024**, *60*, e2023WR035987.

24. Xie, W.; Yin, Q.; Zeng, J.; Yang, F.; Zhang, P.; Yan, B. An improved rock resistivity model based on multi-fractal characterization method for sandstone micro-pore structure using capillary pressure. *Fractal Fract.* **2024**, *8*, 118. [CrossRef]
25. Ge, X.; Fan, Y.; Xing, D.; Xu, Y. A novel method to calculate relative permeability of fluids based on fractal theory and core NMR experiment. *Comput. Model. New Technol.* **2018**, *22*, 87–94.
26. Guo, Y.; Pan, B.; Zhang, L. A new method to identify reservoirs in tight sandstones based on the new model of transverse relaxation time and relative permeability. *Geofluids* **2022**, *2022*, 4820483.
27. Tsakiroglou, C.; Fleury, M. Pore network analysis of resistivity index for water-wet porous media. *Transp. Porous Media* **2000**, *38*, 249–272. [CrossRef]
28. Tong, Q.; He, D.; Xia, Z.; Huang, J.; Di, K.; Xu, F.; Guo, S. Influence of reservoir pore-throat structure heterogeneity on water-flooding seepage: A case study of Yanchang Formation in Ordos Basin. *Minerals* **2022**, *12*, 972. [CrossRef]
29. Pape, H.; Clauser, C.; Iffland, J. Permeability prediction based on fractal pore-space geometry. *Geophysics* **1999**, *64*, 1447–1460. [CrossRef]
30. Zisser, N.; Kemna, A.; Nover, G. Relationship between low-frequency electrical properties and hydraulic permeability of low-permeability sandstones. *Geophysics* **2010**, *75*, E131–E141. [CrossRef]
31. Bakke, S.; Øren, P.E. 3-D pore-scale modelling of sandstones and flow simulations in the pore networks. *SPE J.* **1997**, *2*, 136–149. [CrossRef]
32. Bultreys, T.; Van Hoorebeke, L.; Cnudde, V. Simulating secondary waterflooding in heterogeneous rocks with variable wettability using an image-based, multiscale pore network model. *Water Resour. Res.* **2016**, *52*, 6833–6846. [CrossRef]
33. Gharbi, O.; Blunt, M.J. The impact of wettability and connectivity on relative permeability in carbonates. *Water Resour. Res.* **2012**, *48*, W12513. [CrossRef]
34. Yan, W.; Sun, J.; Dong, H.; Cui, L. Investigating NMR-based absolute and relative permeability models of sandstone using digital rock techniques. *J. Pet. Sci. Eng.* **2021**, *207*, 109105. [CrossRef]
35. Helle, B.; Bhatt, A. Fluid saturation from well logs using committee neural networks. *Pet. Geosci.* **2004**, *10*, 119–127.
36. Wang, Y.; Li, X.; Zhang, L. Transformer-based relative permeability prediction from well logs for heterogeneous sandstone reservoirs. *J. Pet. Sci. Eng.* **2023**, *225*, 111689.
37. Khosravi, R.; Simjoo, M.; Chahardowli, M. Low salinity water flooding: Estimating relative permeability and capillary pressure using coupling of particle swarm optimization and machine learning technique. *Sci. Rep.* **2024**, *14*, 10762. [CrossRef] [PubMed]
38. Zhai, X.; Yu, X.; Zhang, Q.; Bai, L.; Li, X. Low permeability and tight artificial cores preparation under geological conditions. *Adv. Geosci.* **2018**, *8*, 780–787.
39. Han, T.; Huang, T.; He, H.; Fu, L. Slopes of the pressure-dependent elastic–electrical correlations in artificial sandstones. *Geophys. J. Int.* **2024**, *237*, 1010–1020. [CrossRef]
40. Lee, H.; Lee, J.; Oh, T. Permeability evaluation for artificial single rock fracture according to geometric aperture variation using electrical resistivity. *J. Rock Mech. Geotech. Eng.* **2021**, *13*, 827–837. [CrossRef]
41. Maineult, A.; Weller, A.; Martin, T.; Titov, K.; Florsch, N. 3-D impedance networks simulate complex resistivity spectra of sand–pyrite–water mixtures. *Geophys. J. Int.* **2025**, *242*, ggaf269. [CrossRef]
42. Zou, J.; Huo, S.; Liu, E.; Zeng, T.; Hu, L.; Song, Y.; Li, M. Prediction of relative permeability curve based on machine learning driven by logging data. *Appl. Geophys.* **2025**, *12*, 1–13. [CrossRef]
43. Guo, Z.; Zhao, Y.; Liu, Z.; Fan, Q.; Guo, S. Modeling Relative Permeability-Resistivity Relationships from Seepage Experiment Laws. *Appl. Sci.* **2025**, *15*, 8963. [CrossRef]

Disclaimer/Publisher's Note: The statements, opinions and data contained in all publications are solely those of the individual author(s) and contributor(s) and not of MDPI and/or the editor(s). MDPI and/or the editor(s) disclaim responsibility for any injury to people or property resulting from any ideas, methods, instructions or products referred to in the content.